S. Afr. J. Chem., 2015, **68**, 195–200,
<http://journals.sabinet.co.za/sajchem/>.

A Kinetic Insight into the Activation of *n*-Octane with Alkaline-Earth Metal Hydroxyapatites

Venkata D.B.C. Dasireddy, Holger B. Friedrich and Sooboo Singh*

Catalysis Research Group, School of Chemistry and Physics, University of KwaZulu-Natal, Durban, 4000, South Africa.

Received , revised , accepted .

ABSTRACT

Alkaline-earth metal hydroxyapatites are prepared by the co-precipitation method and characterized using XRD, ICP, NH_3-TPD, SEM-EDX, TEM and N_2 physisorption analysis. The metal present in the hydroxyapatite influences the acidity of the catalyst. Oxidative dehydrogenation reactions carried out in a continuous flow fixed bed reactor showed that the selectivity towards desired products was dependent on the alkaline-earth metal in the hydroxyapatite. All hydroxyapatite catalysts showed high selectivity towards carbon oxides, followed by cracked products, octenes and aromatics. The highest selectivity and turnover numbers towards C8 products and a high specific rate was shown by Sr-HAp. The activation of *n*-octane over these catalysts followed the Eley-Rideal mechanism.

KEYWORDS

Hydroxyapatite, acidity, chemisorption, *n*-octane, octenes, aromatics, oxidative dehydrogenation.

1. Introduction

Alkenes are important raw materials in a wide range of applications due to their low cost and ability to be functionalized easily. For over sixty years and until recently, most of the commercial production of alkenes was through the dehydrogenation of alkanes.[1] In these reactions, alkene selectivity is low, temperatures up to 600 °C are required and carbon deposition on the active sites of the catalyst is prevalent.[2] The introduction of oxygen for the activation of alkanes renders the reaction exothermic and reduces carbon deposits on the catalyst. As a result, oxidative dehydrogenation (ODH) of alkanes is preferred and plays an increasing role in the synthesis of alkenes in the chemical industry, especially the petrochemical industry. Our recent studies showed that ODH of *n*-octane over certain heterogeneous catalytic systems yield value-added products such as 1-octene and ethyl benzene.[3] It was also shown that the catalytic performance in these reactions depends on the acid-base properties of the catalyst, in addition to isolated cations capable of activating C-H bonds and sites that can activate the oxygen.[4] Hydroxyapatite (HAp) has acid-base character, offers high stability, allows substitution into the apatite structure and the phosphate groups present in the structure are capable of activating oxygen.[5]

Hydroxyapatite has the general formula,

$$[Ca_{10-x}(HPO_4)_x(PO_4)_{6-x}(OH)_{2-x}, 0 \leq x \leq 1].$$

Stoichiometric HAp has $x = 0$ to give $Ca_{10}(PO_4)_6(OH)_2$, whereas calcium-deficient non-stoichiometric HAp has $0 \leq x \leq 1$.[6] Hydroxyapatites are bifunctional materials with both acidic and basic sites in the crystal lattice and have found applications as catalysts and catalyst supports.[7] They have a hexagonal structure made up from columns of calcium ions and oxygen atoms that are located parallel to the hexagonal axis. Three oxygen atoms from each PO_4 tetrahedron are shared by one column and the fourth oxygen atom is attached to the neighbouring column. The calcium ions in the lattice can be replaced with other cations by ion-exchange, ion-adsorption, dissolution of HAp, followed by deposition of a new phase or a combination of these methods.[8,9] HAp was reported as an efficient catalyst in the catalytic dehydrogenation [10] and in the acid catalyzed decomposition of alcohols.[11] The catalytic efficiency of HAp is enhanced by the impregnation with additional cations. Yamaguchi *et al*.[12] succeeded in creating a monomeric Ru^{3+} species on the surface of HAp which was found to be efficient in the catalytic aerobic oxidation of various alcohols. Recently, titanium substituted HAp was used for the photocatalytic degradation of environmental endocrine disrupting chemicals.[13] The active sites on the hydroxyapatite are the acidic phosphate groups and basic metal atoms. These sites activate oxygen and the resulting oxygen species are directly involved in the abstraction of hydrogen from alkanes, hence, impacting on the rate of the reaction.[14] In this study, we report the preparation and characterization of some alkaline-earth metal hydroxyapatites and assess their efficiency in the catalytic oxidation of *n*-octane.

2. Experimental

2.1. Preparation of Catalysts

Chemicals used in the preparation of the catalysts were purchased from Merck KGa, Darmstadt, Germany. The hydroxyapatites were prepared by the method of Matsumura *et al*.[15] Nitrate salts, $M(NO_3)_2{\cdot}xH_2O$ (6.67×10^{-2} mol) where $M = Ca^{2+}$, Sr^{2+}, Mg^{2+} and Ba^{2+} were dissolved in 60 mL distilled water. The solution was then diluted to 120 mL with distilled water and adjusted to a pH of 11 with aqueous ammonia. A 100 mL solution of $(NH_4)_2HPO_4$ (4.00×10^{-2} mol) was also similarly adjusted to pH 11 and diluted to 160 mL. The phosphate solution was added to the metal solution dropwise over a period of 30 min at room temperature. A gelatinous precipitate formed which was stirred and boiled for 10 min. The solid was filtered, washed to pH 7 with distilled water and dried in air at 110 °C for 12 h, followed by calcination at 550 °C for 6 h in air.

2.2. Characterization of Catalysts

The catalysts were characterized by various physical and chemical methods. The BET surface area and pore volume

* To whom correspondence should be addressed. E-mail: singhso@ukzn.ac.za

ISSN 0379-4350 Online / ©2015 South African Chemical Institute / http://saci.co.za/journal
DOI: http://dx.doi.org/10.17159/0379-4350/2015/v68a26

studies were carried out using a Micrometrics ASAP 2020 multi-point BET surface area analyser. Elemental analysis or chemical composition was performed using inductively coupled plasma (ICP) on a Perkin Elmer Optical Emission Spectrometer Optima 5300 DV. Standards (1000 ppm Ca, Sr, Mg, Ba and P) were purchased from Fluka. The phases present in the catalysts were observed using powder X-ray diffraction (XRD) conducted on a Bruker D8 Advance instrument. Infrared (IR) spectra were obtained using a Perkin-Elmer Precisely Spectrum 100 equipped with a Universal ATR sampling accessory and Raman spectroscopy was carried out using an Advantage 532 series spectrometer (NIR Spectrometer). Ammonia temperature programmed desorption (TPD) and temperature programmed reduction (TPR) studies were carried out using a Micromeritics 2920 Autochem II Chemisorption Analyzer. For TPR experiments, 5 % H2/Ar, flowing at a rate of 30 mL min^{-1}, was used as a reducing agent, whereas for TPD analysis, 4.1 % NH_3/He was passed over the catalyst at a flow rate of 30 mL min^{-1} for 60 min. The amount of oxygen chemisorbed on the surface of hydroxyapatite catalysts was investigated by oxygen chemisorption using a Micromeritics ASAP 2020 chemisorption analyser. Pure oxygen (30 mL min^{-1}) was passed through the sample for 3 h until saturation was obtained. The temperature was ramped from 30 °C up to 500 °C at a ramping rate of 10 °C min^{-1} and the amount of oxygen chemisorbed was measured at this temperature.[16] The surface morphology of the catalysts was obtained using scanning electron microscopy (SEM) **utilizing** a Leo 1450 Scanning Electron Microscope. Transmission electron microscopy (TEM) images were viewed on a Jeol JEM-1010 electron microscope and these images were captured and analyzed using iTEM software.

2.3. Catalytic Testing

Gas phase oxidation reactions were carried out in a continuous flow fixed bed reactor in down flow mode. The catalyst bed (1 mL), comprising pellet sizes between 600 and 1000 μm was located at the centre of the reactor with 24-grit carborundum packed in the spaces on either side of the bed. The *n*-octane feed (Merck, 99 %) was delivered into the system by a high-precision isocratic pump (Lab Alliance Series II). The concentration of *n*-octane in the gaseous mixture was 11 % (v/v) and the *n*-octane to oxygen molar ratio was fixed at 1:1. Air (79 % N_2, 21 % O_2) was used as the oxidant and nitrogen (Afrox, 98 %), the make-up gas to achieve a gas hourly space velocity (GHSV) of 4000 h^{-1}. to obtain an iso-conversion of 8 % (temperature = 500 °C), the GHSV was varied from 3700 to 4250 h^{-1}. Gaseous and liquid products were analyzed off-line using Perkin-Elmer Clarus 400 FID and TCD gas chromatographs. A Perkin-Elmer Clarus 500 GC-MS was used to identify unknown products. Carbon balances ranged between 99 and 101 %. All the data points were obtained in duplicate with an error of ±2 %. The specific reaction rate and the turnover numbers (TON) for the formation of products were calculated as follows:[17]

$$\text{Specific reaction rate} = \frac{(n\text{-octane conversion} / 100)}{(\text{specific surface area of the catalyst} \times \text{GHSV}^{-1} \times 36000} \quad (1)$$

$$\text{Turn over number (TON)} = \frac{\text{moles of the product formed}}{\text{specific surface area of the catalyst}} \quad (2)$$

3. Results and Discussion

3.1. Characterization of Catalysts

The elemental compositions for the catalysts are shown in Table 1. Metal to phosphate ratios (M/P) were in the range of 1.62 to 1.65, suggesting that non-stoichiometric hydroxyapatites were prepared.[18] These results correlated with SEM-EDX elemental analysis.

All the materials showed a similar pattern in the adsorption-desorption isotherms, displaying the characteristic hysteresis loop of a Type IV isotherm (IUPAC) lying in the p/po range of 0.6 to 0.85, demonstrating mesoporous character (Table 1).[19] An inflection observed between the p/p range of 0.85 and 0.95 is attributed to the macropores caused by particle–particle porosity.[20] The catalysts exhibit a step increase at this relative pressure range due to the filling of inter-particle macropores of the catalyst with the nitrogen. The desorption isotherms (Fig. 1) show that the samples have uniform pore size distribution.[21] The surface areas of the hydroxyapatites are in the 40 to 70 m^2 g^{-1} range and are shown in Table 2. From powder XRD (Fig. 2) carried out at room temperature, the d spacing values for 2θ angles between 30 ° and 35 ° correlate with data found in JCPDS File Nos. 9–390, 33–138, 36–0272 and 13–0404 for the calcium, strontium, barium and magnesium hydroxyapatites, respectively, and agrees with data presented by previous researchers.[14,22,23] Mg-HAp showed the highest crystallinity and crystallite size among all the hydroxyapatite catalysts (Table 1). TPR profiles of all the hydroxyapatites showed no peaks, indicating that the hydroxyapatites are stable under a reduction environment.

The TPD studies using NH_3 reveal the existence of both Lewis and Brønsted acidic sites.[21,23] Weak, strong and some moderate acidic sites are attributed to the three peaks present in the TPD profile of the loaded HAp catalysts, at 350–450 °C weak acidic sites, at 450–550 °C moderate acidic sites and above 650 °C strong acidic sites.[24] Lewis acidity is due to the main group metal ions

Table 1 Crystallite size, crystallinity and elemental analysis of alkaline-earth metal hydroxyapatite catalysts.

Catalyst	M/P [a]	M/P [b]	Crystallite size /nm [c]	Crystallinity [d] (X_c)/%	Particle size /nm [e]
Ca-HAp	1.65	1.63	2.90	0.29	168
Sr-HAp	1.62	1.61	3.13	0.30	175
Mg-HAp	1.60	1.62	3.52	0.34	192
Ba-HAp	1.62	1.61	3.10	0.28	182

[a] From ICP (obtained in triplicate with a standard deviation of ±0.04)

[b] From SEM-EDX (obtained in triplicate with a standard deviation of ±0.05)

[c] $X_s = 0.9\lambda/\text{FWHM}\cos\theta$, where X_s is the crystallite size (nm), λ is the wavelength of the monochromatic X-ray beam (λ = 0.15406 nm for Cu$K\alpha$ radiation), FWHM is the full width at half-maximum for the diffraction peak under consideration (radians) and θ is the diffraction angle (degrees)[21].

[d] $X_c = 1 - (V_{112/300}/I_{300})$, where X_c is degree of crystallinity, $V_{112/300}$ is the intensity of the shoulder between the (112) and (300) diffraction peaks and I_{300} is the intensity of the (300) peak[21].

[e] Measured using iTEM software (count of 50–70 particles, with a standard deviation of ±3 nm).

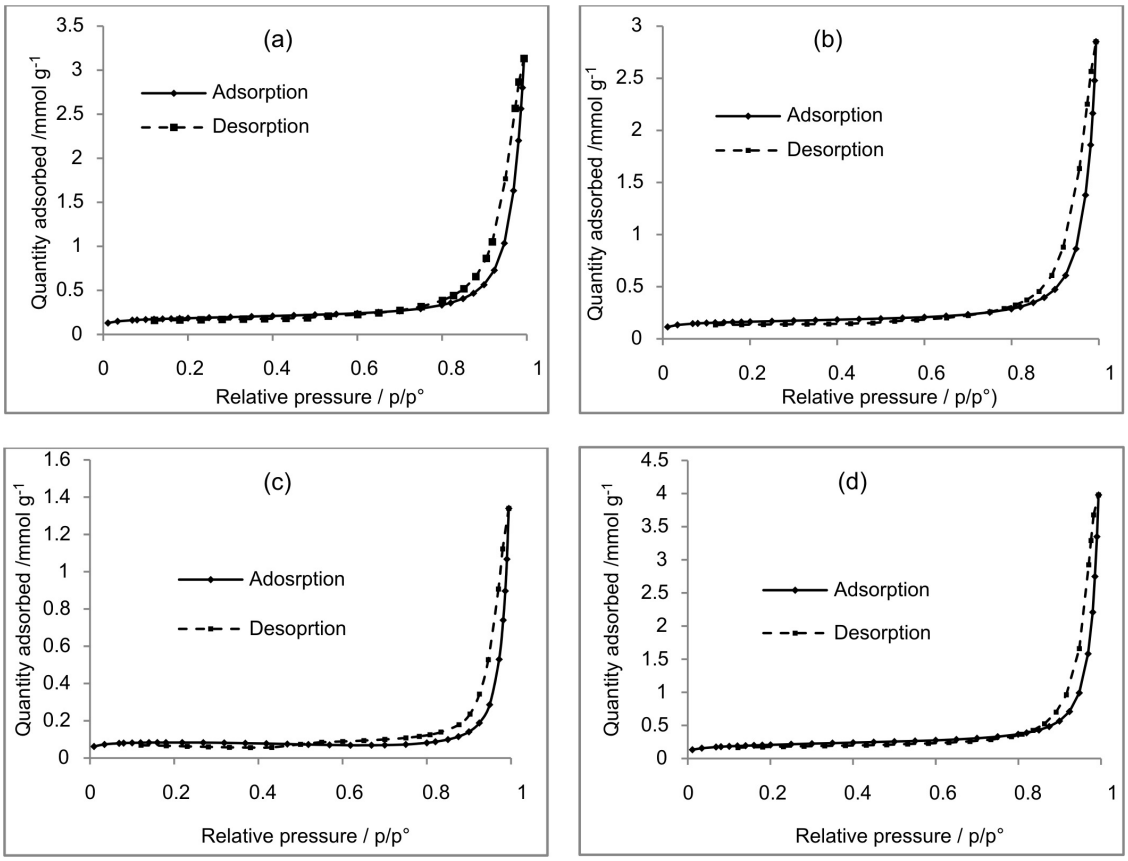

Figure 1 Nitrogen adsorption–desorption isotherms of (**a**) calcium, (**b**) strontium, (**c**) magnesium, and (**d**) barium hydroxyapatite.

Table 2 Physisorption and chemisorption analysis of alkaline-earth metal hydroxyapatite catalysts.

Catalyst	Surface area /$m^2\ g^{-1}$ [a]	Pore volume /$cm\ g^{-1}$ [a]	Average pore size /Å [a]	Average pore width /Å [a]	Oxygen chemisorbed /mmol $O_2\ g^{-1}$ [b]
Ca-HAp	69	0.128	1125	480	27
Sr-HAp	63	0.112	1024	493	39
Mg-HAp	59	0.068	390	610	34
Ba-HAp	42	0.092	220	643	21

[a] Data obtained in duplicate with an error of ±5 % and [b] in triplicate with an error of ±3 %.

present in the hydroxyapatites and the acidity is attributed to the unsaturated hydroxyl groups. High and low specific acidity shown by Sr-HAp and Ca-HAp, respectively, indicates that the acid-base character of the hydroxyapatite catalysts depends on the metal present in the hydroxyapatite (Table 3). Strong acidic sites are seen to dominate in all catalysts. Oxygen chemisorption analysis showed that the metallic surface area is in the range of 22–35 $m^2\ g^{-1}$ for all the catalysts. The capacity of the oxygen chemisorption of the catalysts varies with the metal present on the hydroxyapatite. Among all the hydroxyapatites, Sr-HAp showed greatest tendency to chemisorb oxygen on its surface, followed by Mg-HAp, Ca-HAp and Ba-Hap.

3.2. Catalytic Results

Catalytic testing was carried out over a temperature range of 350 °C to 550 °C with the gas hourly space velocity (GHSV) fixed at 4000, h^{-1}. All catalysts showed an increase in conversion of *n*-octane with an increase in temperature. The high conversion of 13 % was obtained with Sr-HApat 550 °C (Fig. 3) and it was observed that the conversion profile was proportional to the number of acidic sites (Table 3) on the surface of the hydroxyapatites.[21]

There was no contribution towards conversion from redox properties of the catalysts since they are stable under reduction as shown by TPR studies. The conversion is therefore due to the surface oxygen species chemisorbed on the hydroxyapatites.[25] Oxygen chemisorption results are also in agreement with the conversion profiles of *n*-octane. Highest conversion was observed using the Sr-HAp catalyst which showed the highest oxygen chemisorption capacity among all the hydroxyapatite catalysts. Sr-HAp also showed a high specific reaction rate compared to Ca-HAp and Ba-HAp which showed similar specific reaction rates (Table 4). The specific reaction rates are in correlation with the amount of oxygen chemisorbed on the catalysts, thus, it can be inferred that the specific rate of the reaction and the conversion of *n*-octane depends on the amount of oxygen chemisorbed on the catalysts. In addition, the adsorption of *n*-octane on the hydroxyapatites occurs directly from gas-phase. Hence, it is proposed that the activation of *n*-octane over the metal substituted hydroxyapatite catalysts follow the Eley-Rideal mechanism.[26]

A range of octenes and aromatic compounds, cracked products

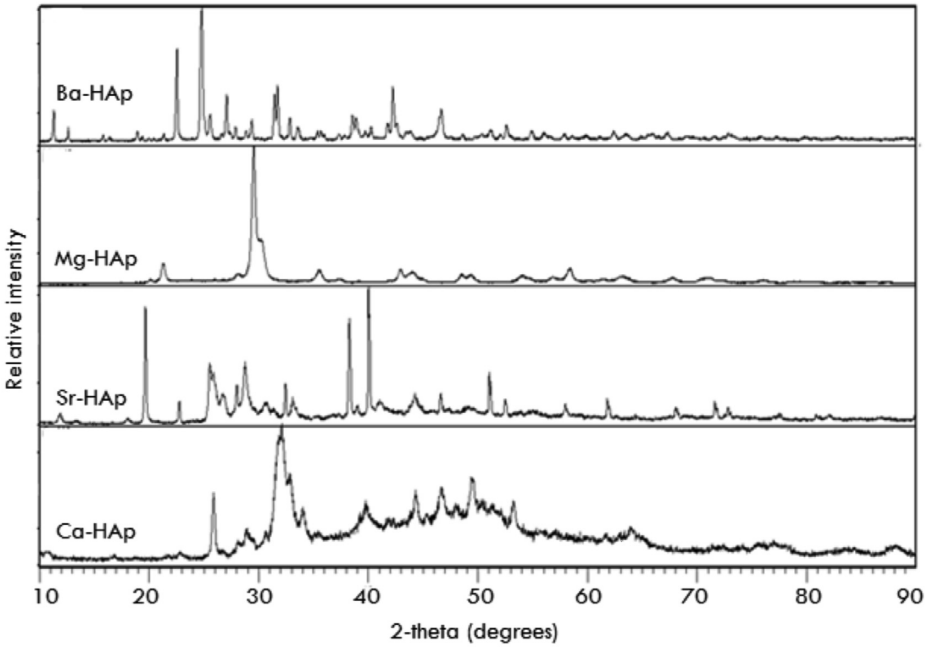

Figure 2 Powder XRD patterns of the alkaline-earth metal hydroxyapatites.

Table 3 NH_3-TPD data of the alkaline-earth metal hydroxyapatite catalysts.

Catalyst	No. of acidic sites[a] /mmol NH_3 g^{-1}			Total acidic sites /mmol NH_3 g^{-1}	Specific acidity /mmol m^{-2}
	Weak (≤450 °C)	Moderate (450–650 °C)	Strong (>650 °C)		
Ca-HAp	68	40	79	187	2.7
Sr-HAp	85	58	99	242	3.9
Mg-HAp	79	48	85	212	3.6
Ba-HAp	51	32	75	158	3.7

[a] Data obtained in duplicate with an error of ±4 %.

and carbon oxides (CO_x) were present in the product stream. Cracked products included mainly ethane, propane, and butane.

Oxygenates were mainly C8 compounds such as octanal, octanol, 2-octanal and 2-octanol. Lower oxygenates such as acetone, acetic acid, propanol and butanol were also present in small amounts. At an iso-conversion of 8 % at 500 °C, carbon oxides are the major product over all the catalysts. The high selectivity towards carbon oxides is probably due to the Brønsted acidity of the catalysts (Table 3). Sr-HAp showed highest selectivity, whereas Ba-HAp showed lowest selectivity towards ODH products, *i.e.* the octenes and aromatics (Fig. 4). This is probably due to the difference in the acidity of the surfaces of Sr-HAp and Ba-HAp and it has been shown that Brønsted acidity favours the formation of aromatics and oxygenates.[21,25]

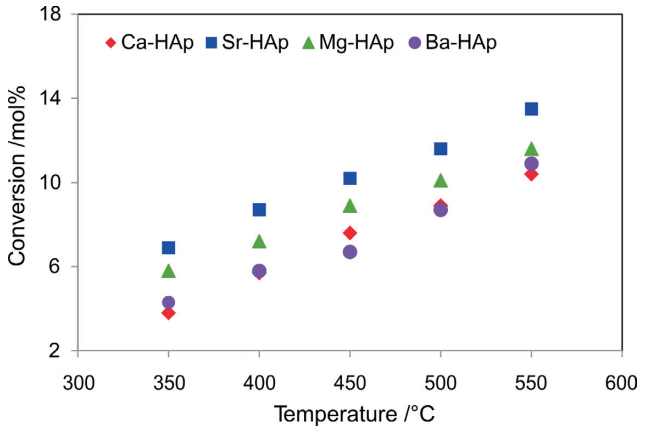

Figure 3 Effect of temperature on *n*-octane conversion over alkaline-earth metal hydroxyapatites (GHSV = 4000 h^{-1}, *n*-octane to oxygen molar ratio of 1:1).

The *cis*- and *trans*-2-octenes (3.6–14.5 %) are the dominant products in the octenes product stream over all the catalysts. The yield towards *trans*-2-octene (2.1–8.4 %) is higher than the *cis*-2-octene (1.5–6.1 %) due to the relative thermodynamic stability of *trans*-isomers compared to the respective *cis*-isomers.[21,25] The yield towards the octene isomers are influenced by the metal present in the hydroxyapatite which determines the extent of the Brønsted acidity of the catalyst.[21] The product profile of octene isomers are similar to the profile observed in previous studies.[21] There is a slight difference in the selectivity towards 1-, 3- and 4-octene, although there is no difference in the energies of the C-H bond at C2, C3 and C4 in the alkane chain. The proposed mechanism for the activation of *n*-octane suggests that the rate determining step is the heterolytic breaking of C-H bonds from the surface alkyl species with the catalyst, followed by a fast elimination of second hydrogen from a neighbouring carbon to form the olefinic bond.[27,28] For cyclization products, *o*-xylene is the dominant product in the aromatics followed by the ethyl benzene and styrene.

o-Xylene is formed *via* C2 to C7 cyclization of 2-octenes and 3-octenes which are the major products in the octene isomers.[21]

Table 4 Specific reaction rate of *n*-octane conversion and turnover number of products (temperature = 450 °C).

Catalyst	Turnover number[a] /10^{-7} mol m^{-2} g^{-1}			Specific reaction rate[a] /10^{-7}mol s^{-1} m^{-2}
	C8 products	Cracked products	CO_x	
Ca-HAp	1.26	0.13	3.22	1.10
Sr-HAp	2.05	0.21	4.56	1.62
Mg-HAp	1.71	0.17	3.85	1.51
Ba-HAp	1.26	0.14	3.37	1.15

[a] Data obtained in duplicate with an error of ±2 %.

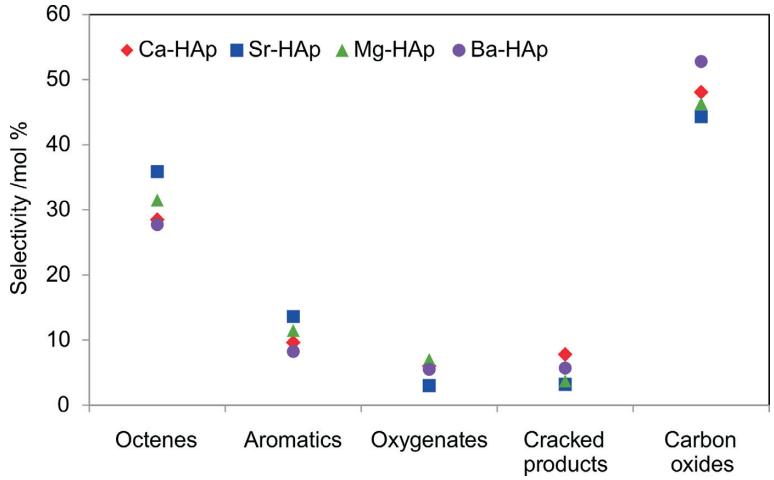

Figure 4 Product selectivity in the activation of *n*-octane over alkaline-earth metal hydroxyapatite catalysts at an iso-conversion of 8 % (GHSV = 3700–4250 h^{-1}, *n*-octane to oxygen molar ratio of 1:1, temperature = 500 °C).

The yield towards the aromatic compounds increased with a subsequent decrease in the octene isomers yield, suggesting that octenes are the precursors for aromatic product formation.[29] Table 4 shows the turnover numbers (TON) of the products formed in the reaction. The TONs of C8 products are in agreement with the acidic and basic character of the catalysts. The relationship between the specific reaction rate and product yield is shown in Fig 5 where the yield towards all products correlate with the specific reaction rate (Table 2).

4. Conclusion

All alkaline-earth metal hydroxyapatite catalysts show mesoporous character, are polycrystalline in nature and are stable under a reducing environment. Conversion profiles of *n*-octane and the specific reaction rates correlates with oxygen chemisorption capacities of the hydroxyapatites and the activation of *n*-octane follows the Eley-Rideal mechanism. The selectivity towards octenes and aromatics is in agreement with the acidic character of the catalysts. The product formation depends on the specific reaction rate which in turn depends on the amount of oxygen chemisorbed on the surface of the catalyst. The strength of the acidity, the highest selectivity towards products and the turnover numbers are in the order:
Sr-HAp > Mg-HAp > Ca-HAp > Ba-HAp.

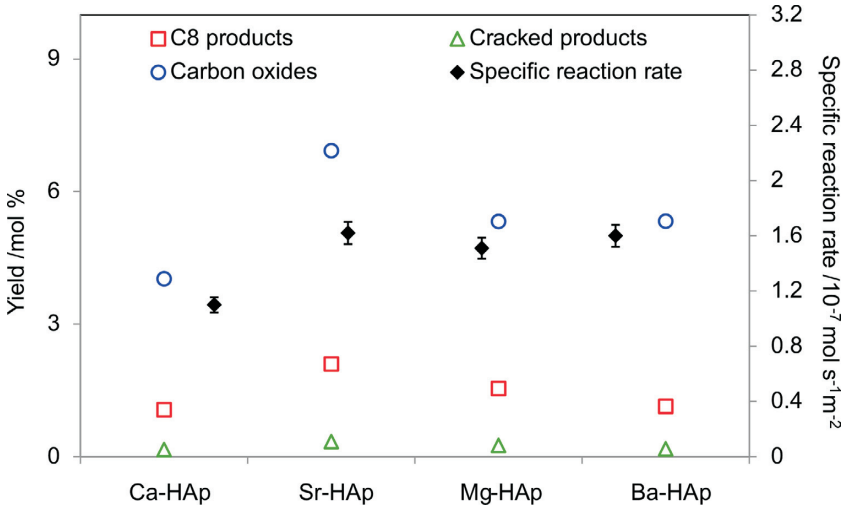

Figure 5 Specific reaction rate of n-octane conversion and yield of products over alkaline-earth metal hydroxyapatite catalysts (GHSV = 4000 h^{-1}, *n*-octane to oxygen molar ratio of 1:1, temperature = 500 °C).

Acknowledgements

We would like to thank the NRF and THRIP for support. Thanks are also extended to the Electron Microscopy Unit at the University of KwaZulu-Natal (Westville).

References

1 H. Zhu, X. Liu, Q. Ge, W. Li, H. and Xu, Production of lower alkenes and light fuels by gas phase oxidative cracking of heavy hydrocarbons, *Fuel Process Technol.,* 2006, **87**, 649–657.

2 M.M. Bhasin, J.H. McCain, B.V. Vora, T. Imai and P R. Pujadø, Dehydrogenation and oxydehydrogenation of paraffins to olefins, *Appl. Catal. A,* 2001, **221**, 397–419.

3 E.A. Elkhalifa, H.B. Friedrich, Oxidative dehydrogenation of n-octane using vanadium-magnesium oxide catalysts with different vanadium loadings, *Appl. Catal. A,* 2010, **373**, 122–131.

4 M. Khachani, M. Kacimi, A. Ensuque, J.-Y. Piquemal, C. Connan, F. Bozon-Verduraz and M. Ziyad, Iron-calcium-hydroxyapatite catalysts: iron speciation and comparative performances in butan-2-ol conversion and propane oxidative dehydrogenation, *Appl. Catal. A,* 2010, **388**, 113–123.

5 S. Sugiyama, T. Osaka, Y. Hirata and K.-I. Sotowa, Enhancement of the activity for oxidative dehydrogenation of propane on calcium hydroxyapatite substituted with vanadate, *Appl. Catal. A*, 2006, **312**, 52–58.

6 S. Sugiyama, T. Miyamoto, H. Hayashi and J.B. Moffat, Effects of non-stoichiometry of calcium and strontium hydroxyapatites on the oxidation of ethane in the presence of tetrachloromethane, *J. Mol. Catal. A: Chem.*, 1998, **135**, 199–208.

7 J.H. Jun, T.H. Lim, S.-W. Nam, S.-A. Hong and K.J. Yoon, Mechanism of partial oxidation of methane over a nickel-calcium hydroxyapatite catalyst, *Appl. Catal., A,* 2006, **312**, 27–34.

8 Z. Opre, J.D. Grunwaldt, M. Maciejewski, D. Ferri, T. Mallat and A. Baiker, Promoted Ru-hydroxyapatite: designed structure for the fast and highly selective oxidation of alcohols with oxygen, *J. Catal.*, 2005, **230**, 406–419.

9 E. Valsami-Jones, K.V. Ragnarsdottir, A. Putnis, D. Bosbach, A.J. Kemp and G. Cressey, The dissolution of apatite in the presence of aqueous metal cations at pH 2–7, *Chem. Geol.,* 1998, **151**, 215–233.

10 H. Monma, Catalytic behavior of calcium phosphates for decompositions of 2-propanol and ethanol, *J. Catal.,* 1982, **75**, 200–203.

11 C.L. Kibby & W.K. Hall, Studies of acid catalyzed reactions: XII. Alcohol decomposition over hydroxyapatite catalysts, *J. Catal*., 1973, **29**, 144–159.

12 K. Yamaguchi, K. Mori, T. Mizugaki, K. Ebitani and K. Kaneda, Creation of a monomeric Ru species on the surface of hydroxyapatite as an efficient heterogeneous catalyst for aerobic alcohol oxidation, *J. Am. Chem. Soc.,* 2000, **122**, 7144–7145.

13 Q. Li, X. Feng, X. Zhang, H. Song, J. Zhang, J. Shang, W. Sun, T. Zhu, M. Wakamura, M. Tsukada and Y. Lu, Photocatalytic degradation of bisphenol A using Ti-substituted hydroxyapatite, *Chinese J. Catal.*, 2014, **35**, 90–98.

14 S. Sugiyama, T. Osaka, Y. Ueno and K.-I. Sotowa, Oxidative dehydrogenation of propane over vanadate catalysts supported on calcium and strontium hydroxyapatites, *J. Jpn. Pet. Inst*., 2008, **51**, 50–57.

15 Y. Matsumura, S. Sugiyama, H. Hayashi, N. Shigemota, K. Saitoh and J.B. Moffat, Strontium hydroxyapatites: catalytic properties in the oxidative dehydrogenation of methane to carbon oxides and hydrogen, *J. Mol. Catal.*, 1994, **92**, 81–94.

16 S.T. Oyama, G.T. Went, K.B. Lewis, A.T. Bell and G.A. Somorjai, Oxygen chemisorption and laser Raman spectroscopy of unsupported and silica-supported vanadium oxide catalysts, *J. Phys. Chem.*, 1989, **93**, 6786–6790.

17 S. Ogo and A. Onda, K. Yanagisawa, Selective synthesis of 1-butanol from ethanol over strontium phosphate hydroxyapatite catalysts, *Appl. Catal. A,* 2011, **402**, 188–195.

18 S. Singh and S. Jonnalagadda, Selective oxidation of n-pentane over V2O5 supported on hydroxyapatite, *Catal. Lett.*, 2008, **126**, 200–206.

19 Y. Kamiya, E. Nishikawa, A. Satsuma, M. Yoshimune and T. Okuhara, Highly porous vanadium phosphorus oxides derived from vanadyl n-butylphosphate, *Microporous Mesoporous Mater.*, 2002, **54**, 277–283.

20 K. Bhattacharyya, S. Varma, A.K. Tripathi, S.R. Bharadwaj and A.K. Tyagi, Effect of vanadia doping and its oxidation state on the photocatalytic activity of TiO2 for gas-phase oxidation of ethene, *J. Phys. Chem. C,* 2008, **112**, 19102–19112.

21 V.D.B.C. Dasireddy, S. Singh and H.B. Friedrich, Activation of n-octane using vanadium oxide supported on alkaline-earth hydroxyapatites, *Appl. Catal. A,* 2013, **456**, 105–117.

22 D. Laurencin, N. Almora-Barrios, N.H. de Leeuw, C. Gervais, C. Bonhomme, F. Mauri, W. Chrzanowski, J.C. Knowles, R.J. Newport, A. Wong, Z. Gan and M.E. Smith, Magnesium incorporation into hydroxyapatite, *Biomaterials,* 2011, **32**, 1826–1837.

23 S. Sugiyama, H. Matsumoto, H. Hayashi and J.B. Moffat, Sorption and ion-exchange properties of barium hydroxyapatite with divalent cations, *Colloids Surf. A,*2000, **169**, 17–26.

24 K.V.R. Chary, G. Kishan, C.P. Kumar and G.V. Sagar, Structure and catalytic properties of vanadium oxide supported on alumina, *Appl. Catal. A,* 2003, **246**, 335–350.

25 V.D.B.C. Dasireddy and S. Singh, H.B. Friedrich, Oxidative dehydrogenation of n-octane using vanadium pentoxide-supported hydroxyapatite catalysts, *Appl. Catal. A,* 2012, **421–422**, 58–69.

26 O. Deutschmann, *Modeling and Simulation of Heterogeneous Catalytic Reactions: From the Molecular Process to the Technical System*, Wiley-VCH, Weinheim, 2013.

27 S. Albonetti, F. Cavani and F. Trifirò, Key Aspects of Catalyst Design for the Selective Oxidation of Paraffins, *Catal. Rev.,* 1996, **38**, 413–438.

28 J.C.Védrine, G.J. Hutchings and C.J. Kiely, Molybdenum oxide model catalysts and vanadium phosphates as actual catalysts for understanding heterogeneous catalytic partial oxidation reactions: a contribution by Jean-Claude Volta, *Catal. Today,* 2013, **217**, 57–64.

29 V.D.B.C. Dasireddy, H.B. Friedrich and S. Singh, Studies towards a mechanistic insight into the activation of n-octane using vanadium supported on alkaline-earth metal hydroxyapatites, *Appl. Catal. A,* 2013, **467**, 142–153.